Effect of Inlet Conditions on Scalar Statistics in Pipe Mixing

James E. Guilkey, Patrick A. McMurtry, and Joseph C. Klewicki
Dept. of Mechanical Engineering, University of Utah, Salt Lake City, UT 84112

Recent experimental validation of theoretical and numerical predictions regarding scalar variance decay in a pipe have revealed that the traditional plug-flow reactor picture of pipe flow omits key physical mechanisms. In particular, the far-field decay exhibits a power law rather than exponential decay. These observations are examined by performing a set of experiments where the manner in which the scalar constituents are introduced into the pipe is varied. Significant differences are noted in the behavior of the variance decay until the very far field is reached, where an invariant power-law form emerges.

Introduction

The study of scalar mixing in a turbulent pipe flow has significant theoretical and practical consequences. Flow in a pipe is a relatively simple configuration, and thus allows fundamental mixing behavior to be explored in a well-characterized flow. Furthermore, pipe mixers are important to industries such as chemical manufacturing and waste processing where in-line devices are often used to enhance mixing. However, such devices often come at the price of significant head loss and substantial installation cost. Exploring the effects of various methods of introducing the species to be mixed can therefore lead to useful insights and have implications in the design of configurations to best promote downstream mixing.

A wide range of studies, with various objectives, have been carried out in turbulent pipe flows. In the pioneering studies of Lee and Brodkey (1964) and Nye and Brodkey (1967), a coaxially located tube was inserted to inject a marker fluid into a turbulent pipe flow. The measured streamwise variance decay exhibited an exponential form, and additional information was provided on the spectral density of the fluctuations. Both sets of their data indicated that initial transients had not relaxed, and the far-field features of the decay could not be deduced. Hartung and Hiby (1972) reported on mixing downstream of a partitioned pipe, each side of which carried a different species. Since then, numerous studies have been made of injecting a jet into the pipe flow for the purposes of optimizing downstream mixing (Ger and Holley, 1976; Fitzgerald and Holley, 1981; Edwards et al., 1985; O'Leary and Forney, 1985; Sroka and Forney, 1989). With the exception of the Hartung and Hiby work, which reported results to about $x/D = 80$, each of these studies only reports on the variance decay of the scalar for a few tens of pipe diameters beyond initialization.

More recently, Kerstein and McMurtry (1994) conducted a theoretical study, backed by stochastic mixing simulations for an idealized configuration in which the length scale of scalar fluctuations was allowed to grow unbounded in one spatial dimension subject to statistically steady stirring. That study revealed two new scaling regimes in the low-wave-number portion of the scalar power spectrum, consistent with their observation of a power-law decay of the scalar variance. It was suggested that a turbulent pipe flow was an appropriate configuration where these predictions could be tested, since the far-field velocity fluctuations are steady, while the scalar fluctuation length scale can grow unbounded in the axial direction.

Motivated by these predictions, Guilkey et al. (1997) carried out a set of experiments specifically designed to match the idealized conditions utilized in the work of Kerstein and McMurtry. In particular, a distinctive inlet condition in which the scalar field was introduced in well-defined blocks (cylindrical blocks with a length equal to the pipe diameter) in a fully developed pipe flow was achieved. The initial flow-field therefore contained scalar and velocity length scales of equal magnitude. Evidence of this narrow-band scalar inlet condition is clearly shown by the spike in the first spectra of Figure 1a. This idealized inlet condition was accomplished using

Correspondence concerning this article should be addressed to J. E. Guilkey.

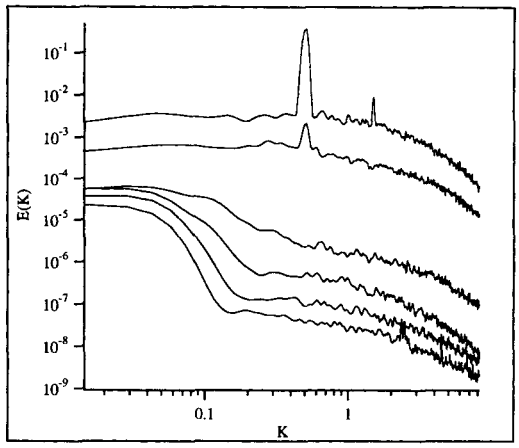

(a)

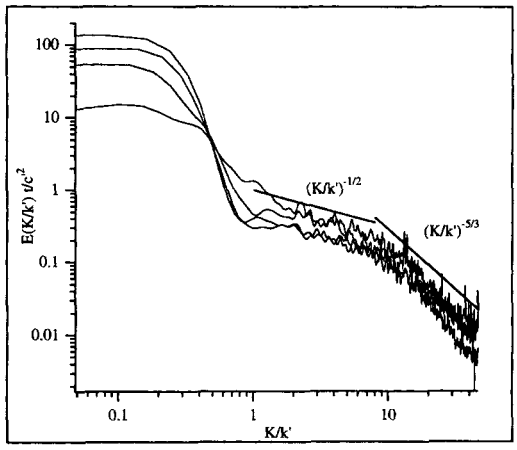

(b)

Figure 1. Power-spectral densities for experiment A: (a) from top to bottom at $x/D = 3.0$, 15.3, 36.8, 53.1, 71.4, and 92.7; (b) far-field at $x/D = 36.8$, 53.1, 71.4, and 92.7 subject to the predicted equilibrium-range scalings.

"caged" fluorescent dyes, as described in Guilkey et al. (1996), and briefly summarized in the next section. Also in Figure 1a are the scalar power spectra for downstream locations to $x/D = 92.7$. The key statistical features of the scalar evolution predicted by the Kerstein and McMurtry work were reproduced experimentally. Namely, in the far field a power-law form of the scalar variance was measured, and at wave numbers below the dominant stirring length scale, the three distinct regimes in the scalar power spectrum were observed (Figures 1a and 1b). (In the following discussion this experiment is referred to as experiment A.) The experimentally measured regimes consisted of a region independent of k, followed by a region of exponential decay up to $k = k'$, where $k' = (\kappa_e t)^{-1/2}/k_v$, and κ_e, t, and k_v are eddy diffusivity, time, and dominant stirring length scale, respectively. (In this and subsequent discussions the wave numbers are nondimensionalized by the dominant stirring length scale, k_v, which corresponds to fluctuations on the order of the pipe diameter.) Finally, for $k' < k < 1$, a $k^{-1/2}$ dependence of the scalar power spectrum was measured. This spectral regime was termed the "equilibrium" regime due to the balance of convective and dissipative mechanisms that give rise to the noted form. [A complete discussion of the details can be found in Kerstein and McMurtry (1994).] The equilibrium regime is followed by the classic $k^{-5/3}$ inertial convective subrange. Higher wave-number regimes (e.g., the k^{-1} viscous–convective subrange) are not resolved due to spatial resolution limitations of the experiments. Although some quantitative differences were noted between the experimentally measured and theoretically derived power-law exponents characterizing the low-wave-number regime, they were shown to result from three-dimensional effects that could not be captured in the theoretical analysis. However, the theoretically determined scalings of the spectra produced the expected collapse of the data in the "equilibrium" regime (Figure 1b). Consistent with these scalings, a power-law form of the variance decay was noted in the far field beyond $x/D > 35$ (Figure 2).

To relate these measured properties to features in the flow, a set of time series of the scalar field at the centerline of the pipe is shown in Figure 3. At a distance of three diameters downstream of the scalar initialization, the coherent blocks of marked and unmarked fluid are still very distinct. By $x/D = 15$ significant mixing has occurred, and high-intensity broad-band fluctuations exist. By $x/D = 36$ (note the change in scale of the vertical axis) the magnitude of the fluctuations has decayed substantially and a low-wave-number component begins to emerge. The high-wave-number fluctuations are dissipated much faster than the low-magnitude, low-wave-number fluctuations. Thus at later times—or at distances farther downstream—the longer wavelength fluctuations constitute the primary contribution to the scalar variance. The transition from exponential to power-law decay is consistent with the emergence of the low-wave-number component of the scalar fluctuations. Physically this occurs because the low-wave-number component decays by a different mechanism than the high-wave-number components. Namely, the high-wave-number components are directly affected by deformations from eddies of size $l_v \leq D$. Eddies of this size do not directly affect the low-wave-number component of the scalar fluctuations, which decays by a less direct turbulent diffusion mechanism—an appropriate mechanism when the scalar fluc-

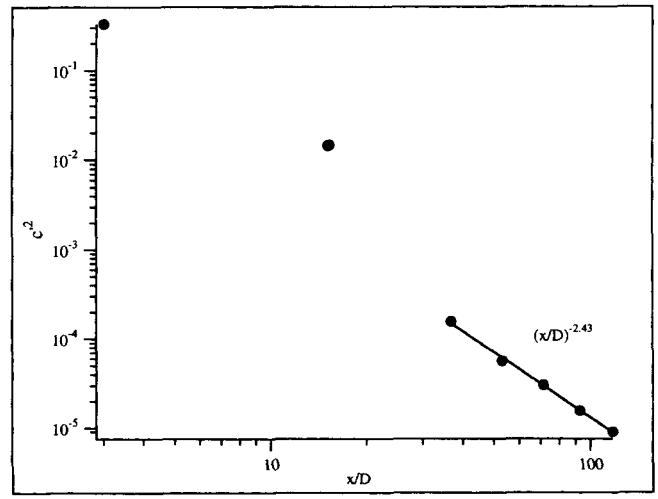

Figure 2. Variance decay for experiment A.

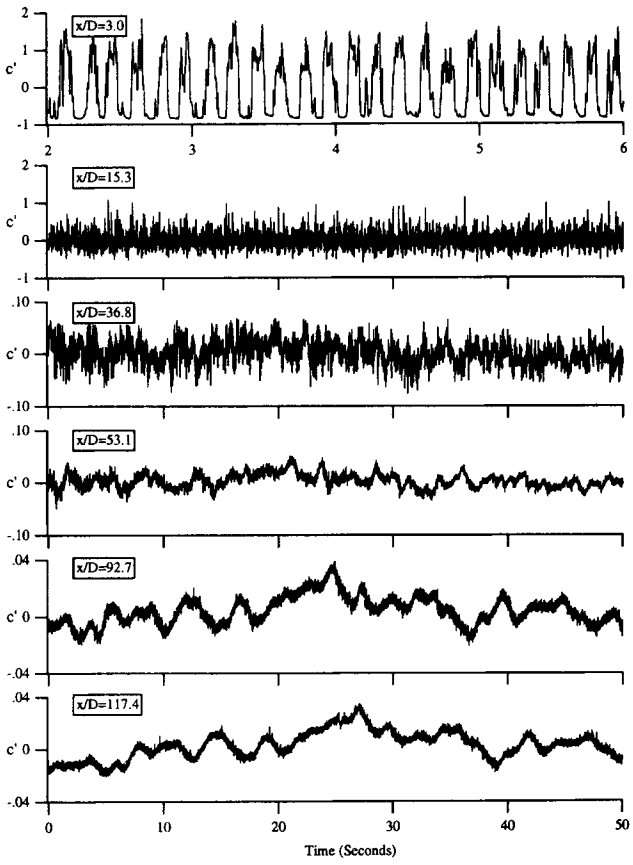

Figure 3. Time series of measured scalar field at the center of the pipe for experiment A.

A 4-s period is shown for $x/D = 3.0$ to show the idealized inlet condition achieved. At all other locations a 50-s time series is shown.

tuation length scale is much larger than that of the velocity length scale. This predicted and measured power-law variance decay is a newly identified feature in pipe flow. It would also seem to contradict previous measurements, including those of Hartung and Hiby, and of Lee and Brodkey and Nye and Brodkey who related their measured exponential variance decay to the predictions of Corrsin (1964). Note however that Corrsin's analysis is only applicable for the decay of scalar fluctuations in an isotropic, turbulent mixer of fixed and finite volume.

Despite the value of the results obtained with experiment A, particularly with respect to the theoretical work by which it was motivated, a number of questions remain. With respect to the results of Hartung and Hiby, who measured the exponential decay of the scalar variance decay out to $x/D = 80$, the effects of inlet conditions need to be explored. To shed light on this issue the physical mechanisms acting in these configurations must be clarified. This raises questions about the generality of the results of experiment A to the variety of more realistic flow conditions encountered in practice. Finally, the implications of these results to design issues must be clarified.

To explore these ideas, results of two additional experiments are reported here. The first (experiment B) is a revisitation of the Hartung and Hiby experiment where measurements are performed over longer downstream distances. The second involves a configuration in which the constituents are introduced into the pipe through a "T" junction. In the following two sections the experimental configuration is described and results presented. A discussion of the different behaviors observed is provided in the Discussion section.

Experimental Configuration

The experimental facility has a 9.75-m-long test section consisting of eight 1.22-m sections of 25-mm-ID quartz pipe, for a total length-to-diameter ratio of about 390. The quartz sections are connected by brass couplers, each of which is fitted with a pressure tap and constructed so as to give a smooth section to section transition. A reservoir, pump, return section and flowmeter complete the flow facility. Total fluid volume of the facility is about 35 L. The passive scalar used in each experiment is fluorescent dye. For each of the experiments the Reynolds number, based on mean velocity and the pipe diameter, is 7,500.

In experiment A the initialization of the scalar field was achieved by using a "caged" or photoactivatable fluorescent dye. This is a dye in which chemical groups have been added to the fluorophores that quench their fluorescent properties. These added groups can be removed by photolysis with a UV photon, thereby regenerating the fluorescent dye. Thus it is possible to introduce a quantity of dye anywhere in the flow field that is accessible to a beam of UV light. Given this ability to introduce dye into the pipe without disturbing the flow, the desired initialization scheme consists of alternating slabs of fluid containing caged and uncaged dye, with the length of each slab approximately equal to the pipe diameter. This initialization is performed at a location approximately 100 pipe diameters downstream of the pipe entrance to assure that the pipe flow is fully developed. The caged dye is insensitive to visible excitation, making it possible to study the mixing between the adjacent blocks of fluid using standard laser-induced fluorescence (LIF) techniques (Koochesfahani and Dimotakis, 1985). The details associated with using photoactivatable fluorophores in mixing studies can be found in Guilkey et al. (1996).

Experiment B reproduces the configuration used by Hartung and Hiby. A 1.33-m section of 25.4-mm-diam. PVC pipe was divided in half along its entire length by a 1.59-mm-thick piece of PVC, which was tapered to a point at the trailing edge. This device, shown in Figure 4, replaced the second quartz section so that the main flow was divided upon enter-

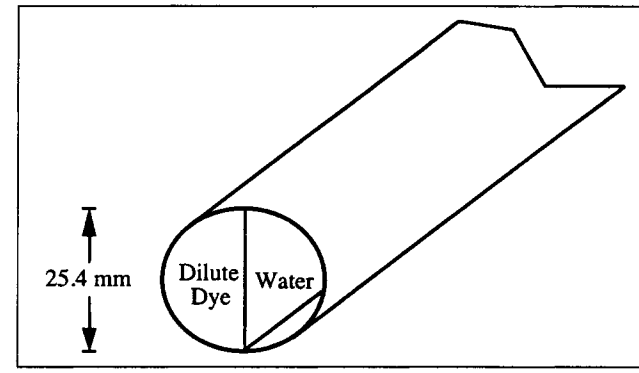

Figure 4. Partitioned pipe inlet.

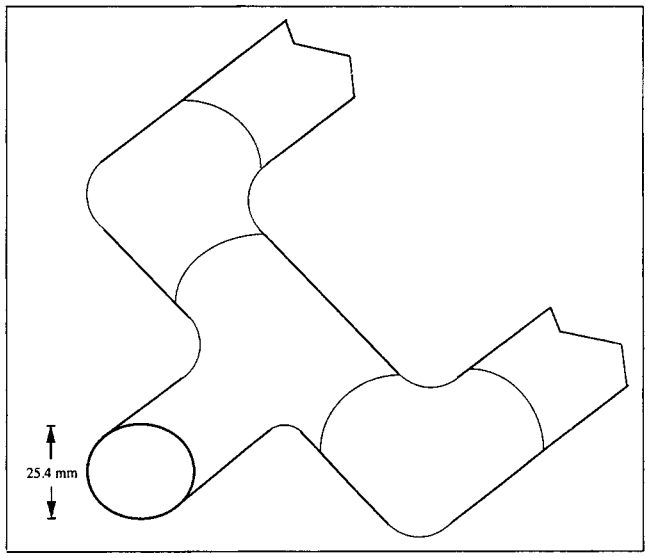

Figure 5. T-junction inlet.

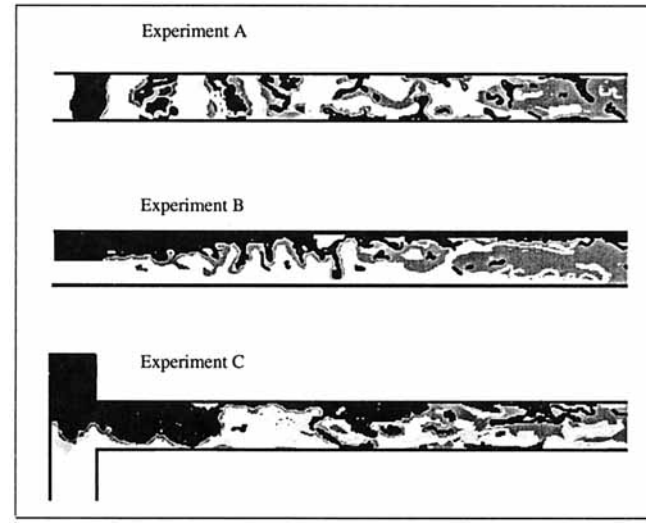

Figure 6. Different 3-D experimental configurations: (a) experiment A; (b) experiment B; (c) experiment C.

ing the mixing region of the pipe. On one side of the divided pipe, dilute fluorescent dye was injected at a rate of approximately 1 L/m using a constant head reservoir located 1.4 m above the test section.

The initialization of experiment C involved two sections of pipe that joined the test section through a T-junction, as shown in Figure 5. The entire device was constructed of 25.4-mm-diam PVC pipe. Again, dilute fluorescent dye was injected into one stream at a rate of approximately 1 L/m from a constant head reservoir. Measurements of the scalar-field fluctuations in the stream containing the dilute dye indicate that the variance of the concentration fluctuations in that stream are less than 0.1% of the fluctuations that result from the interaction of the dye-containing stream with the stream carrying clean water. A two-dimensional representation is provided in Figure 6 to clarify the distinctions among the different experiments.

In each experiment the scalar field is contacted at seven downstream locations using the 488-nm (1.5-W continuous wave) line from an argon ion laser. The single beam from the laser is focused into a custom-built fiber-optic bundle, each leg of which is terminated at a different downstream location. The configuration used is shown in Figure 7. A longpass filter is used to attenuate the scattered laser light while passing the longer wavelength fluorescent light. The filter is positioned between two planoconvex lenses, causing the light to be at normal incidence on the filter. This is the condition for which the filter is designed and thus performs best. The measurement system allows the interrogation of a single point on the centerline of the pipe at each axial location. For the given flow speed, the signal from each photodetector was sampled at 1,000 Hz for up to 120 s, which is approximately the time required for the fluid to make a complete loop. Sampling was achieved with an eight-channel, 16-bit A/D converter interfaced with a UNIX workstation.

The Schmidt number for the dye in the fluid is about 1,900 (Ware et al., 1983) ($Sc = \upsilon/D_m$), where D_m is the molecular diffusivity of fluorescein in water. The Kolmogorov length scale, $\eta = (\epsilon/\upsilon^3)^{1/4}$, was estimated as $\eta = 0.18$ mm at the centerline of the pipe, calculated using an estimate of the dissipation rate ϵ, as reported by Lawn (1971). This corresponds to a Kolmogorov frequency of about 266 Hz ($f_k = U/2\pi\eta$). Thus the sampling rate is well above the Nyquist criterion for resolving the smallest features of the flow field. The factor limiting the resolution of the small structure of the flow was the size of the beam from the fiber optic, which is about 2 mm in diameter, or about 10 Kolmogorov scales. This resolution limitation at high wave numbers does not impact the objectives of the present research, since the issues being investigated are associated with low-wave-number statistics.

Experimental Results

Processing the data involves first normalizing the time series by the mean. This is done to remove the effect of slightly different interrogation laser powers at each of the data-collection locations. The data are then detrended and low-pass filtered. A filter cutoff frequency of 150 Hz is chosen to eliminate the noise and resolution problems that exist at higher frequencies. A power-spectral density (PSD) of the time series is then calculated by breaking the 100+ second data set into 5-s records. Each of these is detrended and the PSD computed. An average PSD is calculated from the ensemble of 5-s records. Use of a large ensemble removes some of the

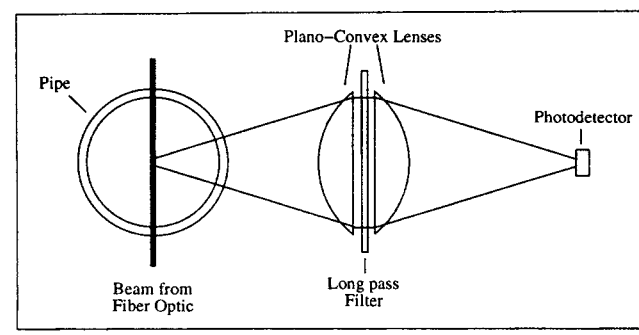

Figure 7. Optical configuration of the scalar interrogation location.

large-scale fluctuations that can be attributed to drift in the laser power or in the photodetector output. A 5-s record, corresponding to 1.5 m for $Re = 7{,}500$, encompasses the wavenumber range accounting for almost all of the scalar variance. The variance, c'^2, is calculated by using a trapezoidal integration algorithm to integrate the PSD.

Experiment B: partitioned pipe

A set of six time series from experiment B, each 50 s long, is shown in Figure 8. One can clearly see the very different nature of the scalar fluctuations as compared to experiment A (Figure 3). Namely, dominance by low-wave-number fluctuations is not seen to develop until $x/D = 109.2$. This is in contrast to experiment A where the emergence of the low-wave-number component appeared by $x/D = 36.8$ and dominates by $x/D = 53.1$. The difference in the spectral content of the fluctuations is reflected in the PSDs, as shown in Figure 9. The emergence of an equilibrium regime is delayed until $x/D = 84.3$. At this point the low-wave-number portion of the PSD has a significantly higher magnitude than at $k = 1$. This is in marked contrast to the PSD shown in Figure 1 for experiment A, in which the emergence of the equilibrium regime is clear by $x/D = 36.8$.

The scalar variance decay for experiment B is shown in Figure 10. An exponential form of the variance decay is apparent, at least as far downstream as $x/D = 80$, at which point the decay becomes slower. The transition to the slower decay appears only after the low-wave-number component of the scalar field develops, which is consistent with the physical

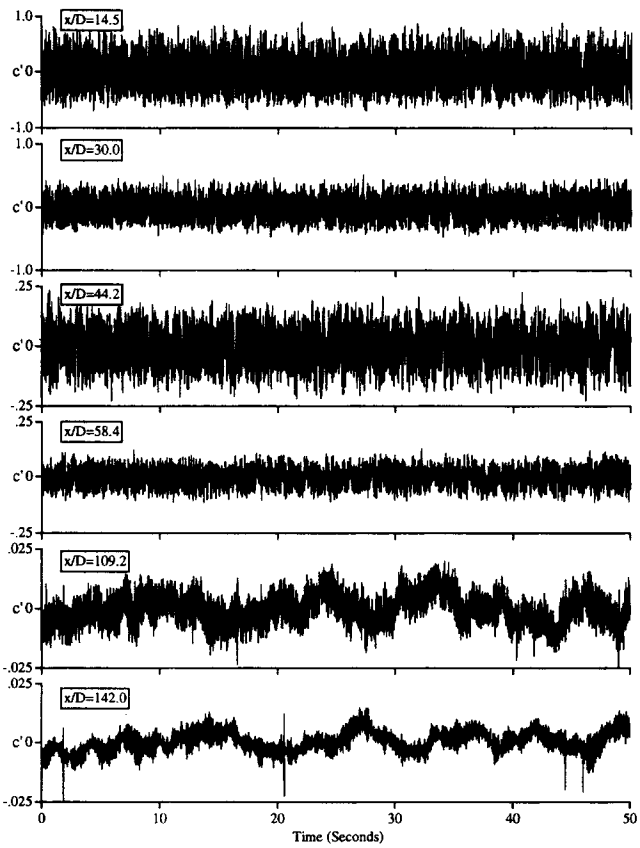

Figure 8. Time series of measured scalar field at the center of the pipe for experiment B.

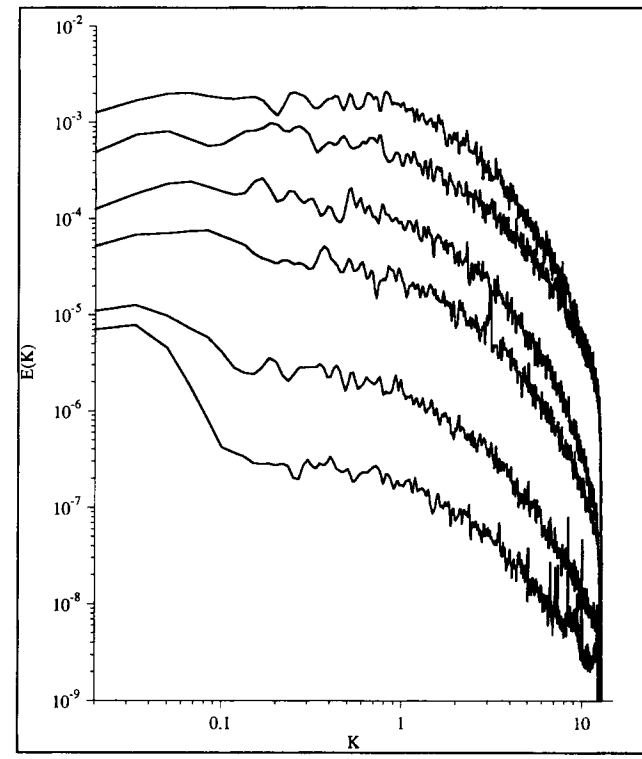

Figure 9. Power-spectral density of scalar fluctuations, experiment B at (from top to bottom) x/D = 14.5, 30.0, 44.2, 58.4, 84.3, and 109.2.

picture described in the Introduction. The predicted equilibrium-range scalings for the PSDs at different downstream locations were found to be delayed in this case. When the spectra were scaled as in Figure 1b, no collapse was observed under the predicted equilibrium-range scaling until the very far field was reached. This is to be expected, as an equilibrium region does not appear until about $x/D = 84.3$.

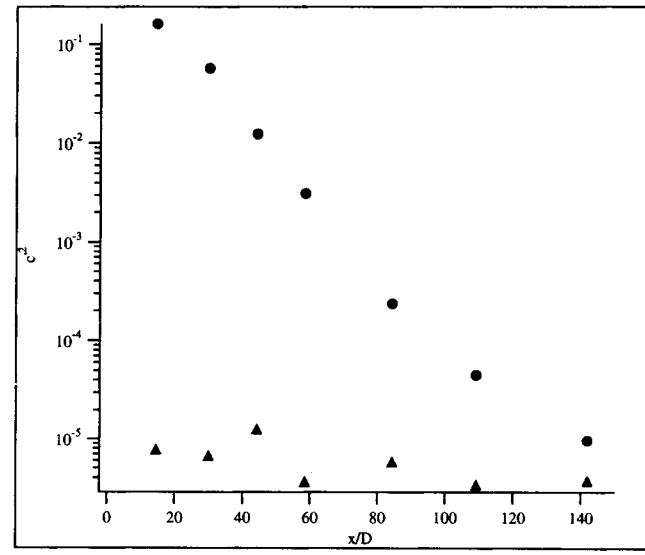

Figure 10. Variance decay, experiment B; the triangles indicate the noise level at each interrogation location.

The key features of experiment B are as follows. The two scalar fields entering the pipe mixing section from a partitioned pipe are initially subject to a wake profile. The scalar field is characterized by a rather broad-band spectrum of fluctuation length scales that decay approximately uniformly up to x/D of about 80. Beyond this, a low-wave-number component is the dominant feature of the scalar fluctuations and the emergence of equilibrium scalings and power-law decay results. Thus, although the near-field mixing behavior is substantially different than in experiment A, the far field evolves to the equilibrium-range scaling predicted by Kerstein and McMurtry. Further discussions of this is provided in the Discussion section.

Experiment C: T-junction

A set of six time series from experiment C, each 50 s in length, is shown in Figure 11. Here again, the time series alone give a substantial indication of the nature of the scalar field. The distinguishing and significant feature revealed in this time series is the appearance of a relatively high-magnitude low-wave-number component at the first measurement location ($x/D = 20.5$ in this case). This is much earlier than in either experiment A or B (compare to Figures 3 and 8). By $x/D = 36$ the scalar fluctuations are completely dominated by the low-wave-number component.

The PSDs of the scalar fluctuations from experiment C, shown in Figure 12, clearly indicate that the low-wave-number fluctuations dominate the variance from the first upstream position measured. In general the behavior of the scalar statistics throughout the domain are very similar to the far-field statistics measured in experiment A. The equilibrium region is well developed by $x/D = 36.0$, and persists to at least $x/D = 148.0$. (The spectra from $x/D = 115.2$ and $x/D = 148.0$ are not shown in Figure 12 due to substantial noise at the high wave numbers that somewhat obscured the other data. Nevertheless, the low-wave-number features demonstrate a continuation of the trends seen upstream of $x/D = 115.2$). The implications of this behavior on the scalar variance decay are given in Figure 13. A power-law decay is noted over the complete domain, with an exponent that is near that measured in the far field of experiment A. It is unclear if the difference between the two exponents is significant, or if a universal power-law exponent may exist. Furthermore, when the equilibrium-range scalings are applied to these spectra, as shown in Figure 14, the collapse that is achieved in the equilibrium region provides further evidence that the scalar fluctuations throughout the pipe behave as those in the far field of experiment A. (Recall k is scaled by k' in this figure, which is proportional to $t^{-1/2}$. The dominant scalar fluctuations thus grow as $t^{1/2}$, consistent with turbulent diffusivity scaling.)

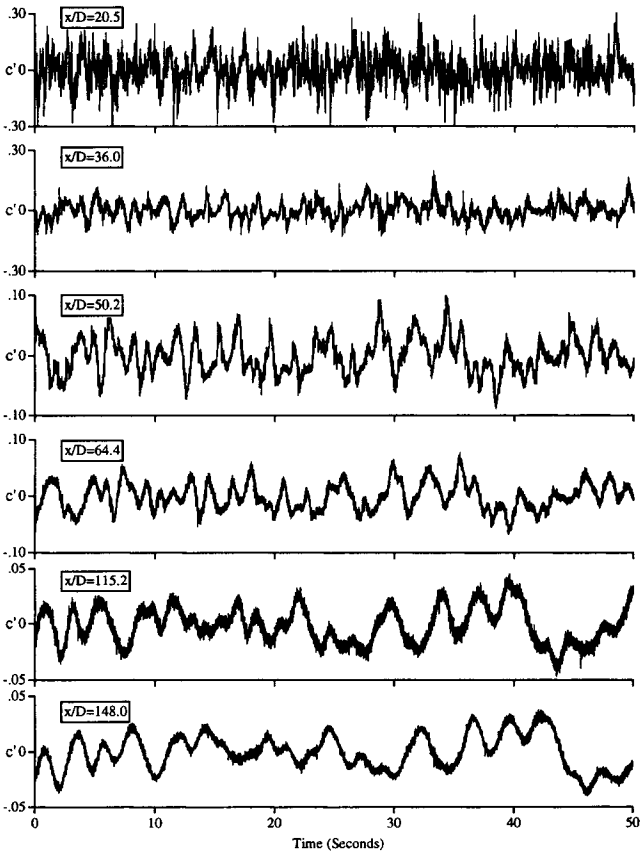

Figure 11. Time series of measured scalar field at the center of the pipe for experiment C.

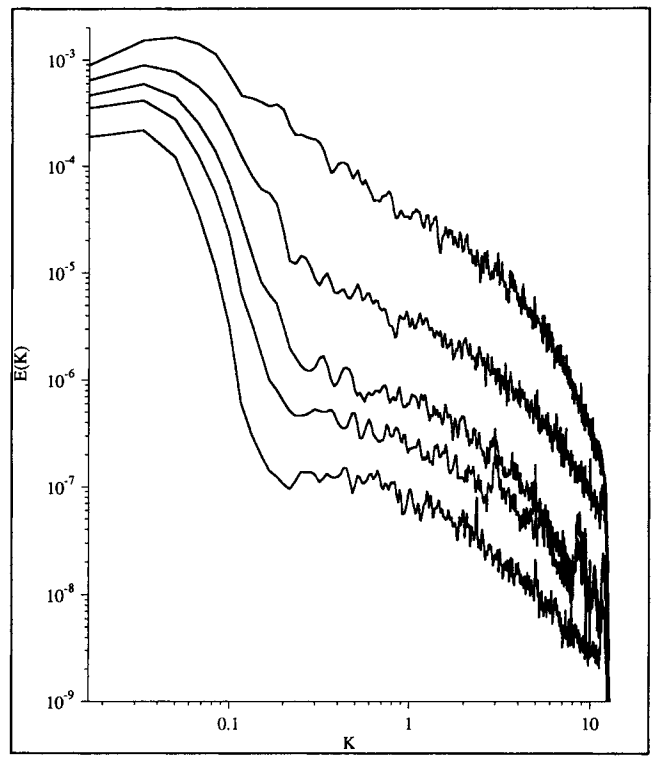

Figure 12. Power-spectral density of scalar fluctuations, experiment C at (from top to bottom) $x/D = 20.5$, 36.0, 50.2, 64.4, and 90.3.

Discussion

All three experiments display important differences in their near-field behavior, yet evolve to a self-similar form in the far field. Several features of this behavior and the differences in the initial mixing mechanisms are noted.

The initial variance decay in experiments A and B are ex-

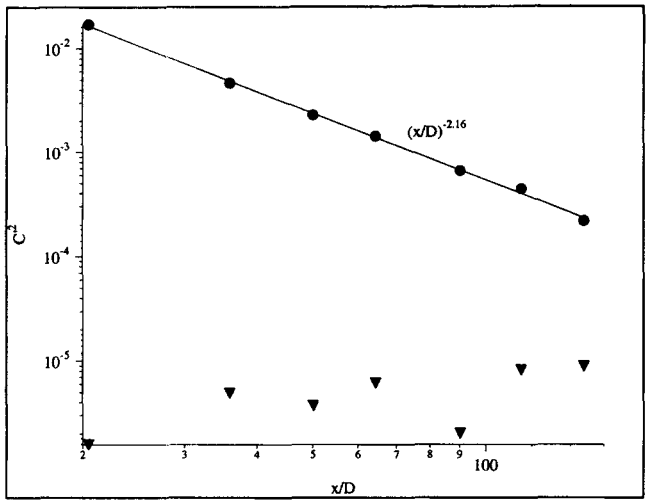

Figure 13. Variance decay, experiment C.

The triangles indicate the noise level at each interrogation location.

ponential. Although the statistical state of the inlet scalar and velocity fields are different, the underlying physical mechanism for this behavior is similar. Prior to development of the low-wave-number components, the dominant velocity scale fluctuations are acting on a scalar field whose fluctuation scale is of the same order. In experiment A both the initial scalar length scale, l_c, and velocity length scale, l_v, are on the order of the pipe diameter, D. In this case, the time scale to break up the fluctuations with length scale of order D is D/u, where u is a characteristic velocity scale in the pipe. The initial decay of the fluctuation magnitude is thus exponential. Measured values give $c'^2 \approx \exp[-0.253x/D]$ for x/D up to about 36. In experiment B, the fluctuation scales are dominated by the evolving wake structure after the partition plate, up to the point where the fully developed velocity profile is attained. In this region both l_c and l_v are confined to the width of the wake. In essence, the mixing behavior can be related to that of a stirred tank whose dimensions are growing with time. In this region an exponential decay is also expected. Note, however, that in experiment B, the decay is of the form $c'^2 \approx \exp[-0.0689x/D]$, that is, an exponential decay, but with a smaller exponent than in experiment A. As noted earlier, the initial mixing time scale in experiment A, where $l_c = D$, is D/u where u is constant. In experiment B, mixing over a length D is not attained until the wake profile has spread across the pipe and a fully developed state is approached.

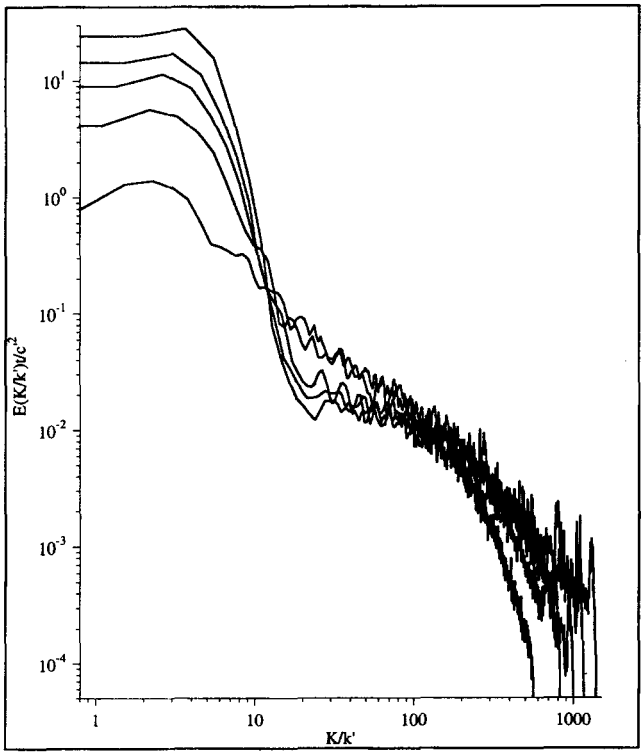

Figure 14. Power-spectral density of scalar fluctuations, experiment B, subject to the predicted equilibrium range scalings.

Axial positions are x/D = 20.5, 36.0, 50.2, 64.4, and 90.3.

The initial mixing behavior in experiment C is much different. From both the time series and PSD it is seen that low-wave-number scalar fluctuations dominate from the first measurement station. This is an effect of the initialization process in which l_c is larger than the stirring length scale $l_v = D$ at the entrance to the pipe. This is attributed here to natural fluctuations in velocity and pressure resulting from the two streams interacting in the T-junction. In this case, small pressure fluctuations in the incoming streams can result in periodically varying contributions to the main pipe flow from the two streams. The time series of experiment C (Figure 11) appear to confirm this picture. As a result, the velocity field acts on scalar fluctuations where $l_c > l_v$ throughout the complete mixing region. The result is a power-law decay from the first measurement location.

It is interesting to note that the "crudest" of the three experiments (experiment C) provides the "cleanest" demonstration of the scaling laws predicted in the Kerstein–McMurtry analysis. This is primarily due to the early presence of a low-wave-number component that allows subsequent downstream measurements to be made with higher signal-to-noise ratios. In all three cases, the development of a low-wave-number component eventually appears and the transition to the slower power-law decay follows.

Finally it is noted that no discrepancy exists between the measurements of Hartung and Hiby and the pipe-flow measurements reported here. Experiment B reproduces the behavior of the Hartung–Hiby experiment over the spatial domain in which their measurements were made. The self-similar far-field state was not observed there due to the limited range of x/D over which their measurements were made. The same is true of the Lee and Brodkey and Nye and Brodkey experiments. Rather than a wake created by a splitter plate, they measured mixing downstream of a wake created by a coaxial tube, the wake separating the two species to be mixed. Again, given the limited range of x/D over which their measurements were made, the self-similar state could not be observed.

Conclusions

The results of this study demonstrate that

- Power-law decay of the scalar variance is a generic feature in the far field of pipe flow.

• A similarity scaling of the power spectrum emerges independent of inlet conditions after flow-field development effects have died out.

• The initial mixing rate (both quantitative and qualitative) in pipe flow is strongly influenced by the manner in which the constituents are introduced into the pipe. In particular, simple changes in flow conditions can have significant effects on the mixing rate.

• Once low-wave-number fluctuations are in place, they are slow to be dissipated by stirring at the advection length scale.

These observations reinforce previous observation (Guilkey et al., 1997) that the traditional picture of pipe flow mixing in the context of a stirred reactor convecting at the mean velocity omits the key mechanisms responsible for far-field similarity scalings.

Acknowledgments

This work was supported by the National Science Foundation under grant CTS 9258445. Facilities and support of the Advanced Combustion Engineering Research Center at the University of Utah and Brigham Young University are gratefully acknowledged. The combustion center receives support from the National Science Foundation, the State of Utah, and 26 industrial participants. The authors thank Alan Kerstein for suggesting these experiments and for insightful discussion of the results, and Lisa Hansen for helping to collect and analyze the data.

Literature Cited

Corrsin, S., "The Isotropic Turbulent Mixer: Part ii. Arbitrary Schmidt Number," *AIAA J.*, **10**, 870 (1964).

Edwards, A. C., W. D. Sherman, and R. E. Breidenthal, "Turbulent Mixing in Tubes with Transverse Injection," *AIChE J.*, **31**, 516 (1985).

Fitzgerald, S. D., and E. R. Holley, "Jet Injections for Optimum Mixing in Pipe Flow," *J. Hydraul. Div. ASCE*, **107**, 1179 (1981).

Ger, A. M., and E. R. Holley, "Comparison of Single-point Injections in Pipe Flow," *J. Hydraul. Div. ASCE*, **102**, 731 (1976).

Guilkey, J. E., K. R. Gee, P. A. McMurtry, and J. C. Klewicki, "Use of Caged Fluorescent Dyes for the Study of Turbulent Passive Scalar Mixing," *Exp. Fluids*, **21**, 237 (1996).

Guilkey, J. E., A. R. Kerstein, P. A. McMurtry, and J. C. Klewicki, "Mixing Mechanisms in Turbulent Pipe Flow," *Phys. Fluids*, **9**, 717 (1997).

Hartung, K. H., and J. W. Hiby, "Beschleunigung der Turbulenten Mischung in Rohren," *Chem. Ing. Tech.*, **44**, 1051 (1972).

Kerstein, A. R., and P. A. McMurtry, "Low-Wave-Number Statistics of Randomly Advected Passive Scalars," *Phys. Rev. E*, **50**, 2057 (1994).

Koochesfahani, M. M., and P. E. Dimotakis, "Laser-induced Fluorescence Measurements of Mixed Fluid Concentration in a Liquid Plane Shear Layer," *AIAA J.*, **23**, 1700 (1985).

Lawn, C. J., "The Determination of the Rate of Dissipation in Turbulent Pipe Flow," *J. Fluid Mech.*, **48**, 477 (1971).

Lee, J., and R. S. Brodkey, "Turbulent Motion and Mixing in a Pipe," *AIChE J.*, **10**, 187 (1964).

Nye, J. O., and R. S. Brodkey, "The Scalar Spectrum in the Viscous-Convective Subrange," *J. Fluid Mech.*, **29**, 151 (1967).

O'Leary, C. D., and L. J. Forney, "Optimization of In-line Mixing at a 90 Degree Tee," *Ind. Eng. Chem. Process Des. Dev.*, **24**, 332 (1985).

Sroka, L. M., and L. J. Forney, "Fluid Mixing with a Pipeline Tee: Theory and Experiment," *AIChE J.*, **35**, 406 (1989).

Ware, B. R., D. Cyr, S. Gorti, and F. Lanni, *Measurement of Suspended Particles by Quasi-elastic Light Scattering*, Wiley, New York (1983).

Manuscript received Dec. 6, 1996, and revision received March 31, 1997.